




**Qudits for witnessing quantum-gravity-induced entanglement of masses under decoherence**Jules Tilly <sup>1,\*</sup>, Ryan J. Marshman <sup>1</sup>, Anupam Mazumdar,<sup>2</sup> and Sougato Bose<sup>1</sup><sup>1</sup>*Department of Physics and Astronomy, University College London, London WC1E 6BT, United Kingdom*<sup>2</sup>*Van Swinderen Institute, University of Groningen, 9747 AG Groningen, Netherlands* (Received 3 February 2021; revised 3 September 2021; accepted 7 September 2021; published 15 November 2021)

Recently, a theoretical and an experimental protocol known as quantum-gravity-induced entanglement of masses (QGEM) has been proposed to test the quantum nature of gravity using two mesoscopic masses, each placed in a superposition of two locations. If after eliminating all nongravitational interactions between them the particles become entangled, one can conclude that the gravitational potential is induced via a quantum mediator, i.e., graviton. In this paper we explore extensions of the QGEM experiment to multidimensional quantum objects and examine a range of different experiment geometries, in order to determine which would generate entanglement faster. We conclude that when a sufficiently high decoherence rate is introduced, multicomponent superpositions can outperform the two-qubit setup. With low decoherence however, and given a maximum distance  $\Delta x$  between any two spatial states of a superposition, a set of two qubits placed in spatial superposition parallel to one another will outperform all other models given realistic experimental parameters. This is further verified with an experiment simulation, showing that  $O(10^3)$  measurements are required to reject the no-entanglement hypothesis with a parallel-qubit setup without decoherence at a 99.9% confidence level. The number of measurements increases when decoherence is introduced. When the decoherence rate reaches 0.125 Hz, six-dimensional qudits are required as the two-qubit system entanglement cannot be witnessed anymore. However, in this case,  $O(10^6)$  measurements will be required. One can group the witness operators to measure in order to reduce the number of measurements (up to tenfold). However, this may be challenging to implement experimentally.

DOI: [10.1103/PhysRevA.104.052416](https://doi.org/10.1103/PhysRevA.104.052416)**I. INTRODUCTION**

Testing the quantum aspect of gravity is a central question of modern physics. While many theories of quantum gravity have been developed, there remains no consensus on how to unify the theories of general relativity and quantum physics. However, the lack of experimental evidence for gravity being quantum still remains an impediment in ongoing research [1].

A number of recent experimental proposals have focused on trying to unveil general-relativity (GR) and post-GR evidence [2–10] and there has also been an initial attempt to rule out the semiclassical treatment of quantum gravity in [11]. Even attempts of detecting the *B*-mode polarization of stochastic gravitational waves have uncertainties in the initial conditions for the universe, which does not provide a concrete test for the quantum nature of gravity [12].

In this regard, there has been recent progress in providing a razor-sharp witness to test the existence of the quantum nature of a graviton in a tabletop experiment based on the following observations [13].

(i) The mediator of the universal gravitational interaction occurs via a spin-2 massless graviton, and if the graviton is quantum, it will entangle the two or more quantum matter states and provide the static gravitational potential at the lowest order in the graviton/matter loop expansion.

(ii) The above statement strictly relies on two main assumptions: special relativity and perturbative quantum field

theory, which allows an off-shell/virtual exchange of a graviton to mediate the gravitational force.

Based on this, a bona fide test for the quantum nature of the gravitational interaction was proposed in [14], where the two mesoscopic masses were allowed to interact in a spatially superposed quantum state via gravity. A similar proposal was also made in [15]. This has attracted significant interest from the research community [16–31] and an experimental initiative in creating a macroscopic superposition with the Stern-Gerlach setup [32]. The above proposal has been coined quantum gravity-induced entanglement of masses (QGEM), which exploits the loophole that as local operations and classical communications are unable to entangle the two quantum states if they are not entangled, to begin with, quantum communication is required to generate the entanglement as highlighted in [13]. The locality is required for making local measurements. However, a nonlocal gravitational interaction [33,34] is indeed allowed to entangle the two quantum states of matter as shown in [13].

This paper extends the QGEM experiment by analyzing a version in which multicomponent superposition beyond qubits is allowed (three, qutrits; *D*, qudits). In addition, we analyze different possible setups for the QGEM proposal in order to determine which will be most efficient to implement in a real experiment. In particular, we consider how quickly different setups can generate entanglement according to a generalized model of the QGEM experiment and how many measurements would be required to witness that entanglement. We test our findings in the presence of decoherence, furthering the analyses presented in [19–22].

\*jules.tilly.18@ucl.ac.uk

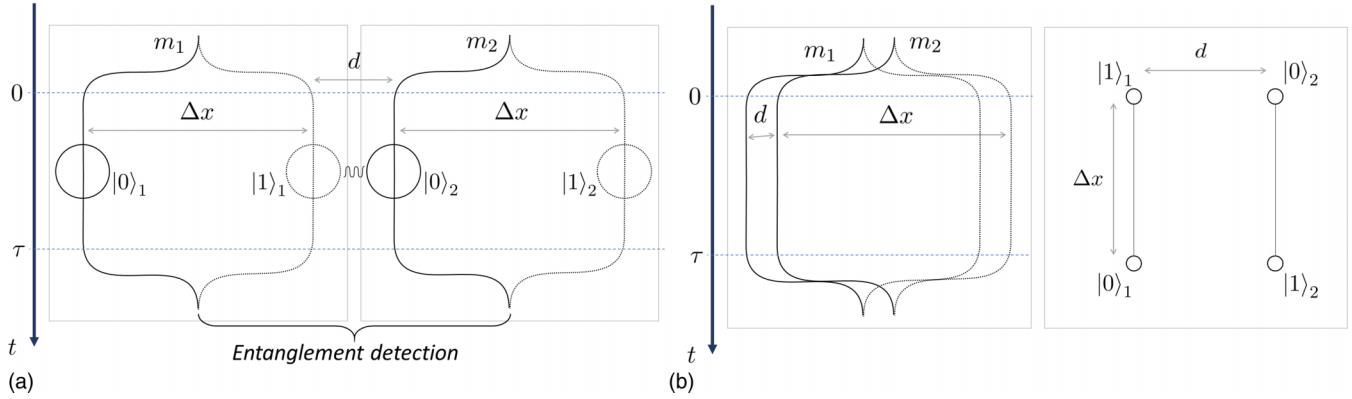


FIG. 1. Schematic representation of the experiment, shown here using qubits: (a) the linear setup presented in [14,15,21] and (b) a schematic for the parallel setup initially presented in [20].

Our key findings are that the parallel setups [20] of the experiment entangle faster than any other setup considered; in the presence of decoherence, using qudits may be beneficial for the experiment and could even be necessary; we provide an order of magnitude for the number of measurements required to reach a 99.9% level of confidence (about  $3.4\sigma$ ) for different decoherence rates (up to 0.125 Hz).

This paper will proceed as follows. Section II presents a generalized version of the QGEM experiment, with arbitrary geometries and allowing for the use of spatial qudits. In Sec. III we analyze the different setups proposed using the entanglement entropy under the assumption of no decoherence. More practical entanglement witnesses are introduced in Sec. IV and used to reanalyze the experiment allowing for decoherence in Sec. V. A statistical simulation of the results is presented in Sec. VI to demonstrate how the required number of runs varies with the dimension of the qudits and the decoherence rate assumed.

## II. QGEM WITH QUDITS

The QGEM experimental protocol [14,21] ensured that the gravitational interaction would dominate over the electromagnetic interactions and the Casimir induced vacuum fluctuations. This also provides one of the primary constraints on the experimental setup, which we will not seek to modify in this paper. Specifically, there must be some minimum distance  $d$  maintained between the two particles. A schematic of two potential forms of the experiment is presented in Fig. 1.

The superposition width (or distance between the leftmost and the rightmost superposition instance of each qubit) is labeled  $\Delta x$  and was originally suggested to be approximately  $250 \mu\text{m}$  [14]. While the superposition is held, the qubits are maintained at a distance such that their innermost superposition instances are a least  $d$  apart (with  $d \sim 200 \mu\text{m}$  [14]). If  $d < 200 \mu\text{m}$  then forces such as Casimir-Polder forces and van der Waals forces can affect the overall state of the system: Gravity is no longer the only possible quantum mediator for interactions between the two objects. There has been further work considered to mediate this (see, for instance, [21]); however, as it is beyond the primary considerations here and it does not affect any final conclusion, we will not include it here.

The two qubits are held in this superposition state for a time  $\tau$  ([14] suggests  $\tau = 2.5 \text{ s}$ ) after which the spatial states are brought together. The qubits are then measured to determine whether they were entangled by their gravitational interactions during the superposition period.

Nguyen and Bernards proposed a nearly identical scheme [20], in which the superposition positions of each qubit are aligned parallel to each other as opposed to linearly as in [14,21]. A schematic for this can be found in Fig. 1. This scheme was motivated by the fact that maintaining the distance between the two qubits would be easier in the parallel case than in the linear case.

In the remainder of this paper, we take the experimental parameters to match those proposed by Bose *et al.*, that is,  $d$  is always set to approximately  $200 \mu\text{m}$  and the masses of the two qudits are always approximately  $10^{-14} \text{ kg}$ . Furthermore, unless otherwise stated  $\Delta x \sim 250 \mu\text{m}$ .

While both [14,20] have discussed the implementation of the respective setups, none of the intermediary models have been considered and no direct comparison has been drawn with respect to their impact on how fast the qubit pair entangles or whether qudits would result in faster entanglement.

We present a generalized model for the QGEM experiment, considering rotations of each interferometer, centered on the innermost spatial states of the two qudits (see Fig. 2). The allowed space of the rotation angles  $\theta_1$  and  $\theta_2$  must be restricted so that at no point do the two masses come within a distance  $d$  of one another. The linear setup and the parallel setup are special cases of the above, using the angles  $\theta_1 = \theta_2 = 0$  and  $\theta_1 = \frac{3\pi}{2}$ ,  $\theta_2 = \frac{\pi}{2}$  respectively.

Our model also allows for the use of qudits, rather than qubits, that is, using  $D$  spatial superposition states (and equivalently spin states, assuming Stern-Gerlach interferometry is used as previously proposed) where  $D \geq 2$ ,  $D \in \mathbb{N}$ . Under these conditions, the generalized state of the system resulting from the QGEM experiment can be written as

$$|\psi(t = \tau)\rangle = \frac{1}{D} \sum_{p=0}^{D-1} \left( |p\rangle \otimes \sum_{q=0}^{D-1} e^{i\phi_{pq}} |q\rangle \right), \quad (1)$$

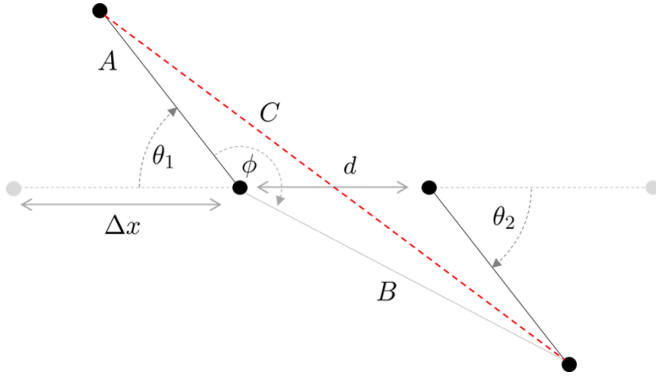


FIG. 2. Top view for the generalized QGEM model showing the maximum spread of the qudits (distance  $C_{pq}$  in red). The parametrization of the setup is controlled by  $\theta_1$  and  $\theta_2$ .

where  $\phi_{pq}$  is defined by

$$\phi_{pq} \sim \frac{Gm_1 m_2 \tau}{\hbar C_{pq}}. \quad (2)$$

The value  $C_{pq}$  for each superposition pair can be derived using simple trigonometric rules and is given by

$$C_{pq} = \sqrt{A_p^2 + B_q^2 - 2A_p B_q \cos(\theta_3)}, \quad (3)$$

where

$$A_p = [(D-1) - p] \frac{\Delta x}{(D-1)}, \quad (4)$$

$$B_q = \left[ d^2 + \left( q \frac{\Delta x}{(D-1)} \right)^2 - 2d \left( q \frac{\Delta x}{(D-1)} \right) \cos(\pi - \theta_2) \right]^{1/2}, \quad (5)$$

$$\theta_3 = \pi - \theta_1 + \arcsin \left( \frac{q \frac{\Delta x}{(D-1)} \sin(\theta_2)}{B_q} \right). \quad (6)$$

### III. ENTANGLEMENT ENTROPY TEST

To assess different setups for the QGEM experiment, we begin by comparing the von Neumann entropy, or entanglement entropy, of the output state. We recall that denoting by  $\rho_1$  the partial trace over the first qudit of the two-qudit system  $\rho$ , the entanglement entropy is given by [35]

$$S(\rho) = -\text{Tr}(\rho_1 \log_2 \rho_1) \quad (7)$$

or, using the eigendecomposition of  $\rho_1$ ,  $\rho_1 = \sum_j \lambda_j |j\rangle\langle j|$ , we can rewrite  $S(\rho)$  as

$$S(\rho) = -\sum_j \lambda_j \log_2(\lambda_j). \quad (8)$$

For a  $D$  level system, the von Neumann entropy is bound by

$$0 \leq S(\rho) \leq \log_2(D), \quad (9)$$

from which it follows that more entanglement can be produced from higher-dimension systems. However, this does not provide any information on how quickly such entanglement is created. Here we focus on the linear and parallel setups;

a discussion regarding all other alternatives is presented in Appendix A.

In order to assess whether qubits perform better or worse than higher-dimensional qudits, we compute the entanglement entropy for  $\rho_{\text{para}}$  and  $\rho_{\text{lin}}$  using the generalized version of the model for two- to six-dimensional qudits. The resulting entropy scaling with time is plotted in Fig. 3. The parallel setup appears to perform significantly better than the linear setup in realistic experiment times.

At the proposed experimental time of 2.5 s, the parallel-qubit case achieves an entanglement entropy of 0.152, much larger than that for the qutrit case of 0.084. Going to higher dimensions further reduces the entanglement entropy to 0.068, 0.060, and 0.056 for four, five, and six dimensions, respectively,<sup>1</sup> suggesting that, under this model, multicomponent superpositions do not entangle faster through gravity. Of course, given that the superposition phases for the state resulting from the QGEM experiment are periodic, the linear setup will achieve a higher entanglement entropy than the parallel setup for sufficiently long experiment times.

The entanglement entropy is not a valid metric for entanglement if classical mixing or decoherence is affecting the system as these are indistinguishable from entanglement as a source of entanglement entropy. Therefore, entanglement entropy is only used when assuming the system is at all times in a pure state. As such, for more realistic experiments, it is necessary to consider other methods of witnessing the entanglement.

### IV. ENTANGLEMENT WITNESS TESTS

Multiple external factors can affect the system state throughout the experiment; these include decoherence and classical uncertainties introduced by the hardware used to implement the experiment. Entanglement witnesses provide a convenient testing system in the context of an experiment.

The positive partial transpose (PPT) entanglement witness is an appropriate witness for two negative partial transpose (NPT) entangled qudits:

$$\mathcal{W}_{\text{PPT}} = |\lambda_{-}\rangle\langle\lambda_{-}|^T. \quad (10)$$

In the parallel-qubit case, this witness is simply [19]

$$\mathcal{W}_{\text{PPT}} = \frac{1}{4}[\mathbb{I} - X \otimes X - Z \otimes Y - Y \otimes Z]. \quad (11)$$

It is worth noting however that although this witness is not optimal in the linear setup, having fewer terms to measure results in less variance when conducting the experiment (for a given number of measurements) (see Sec. VI). In addition, all of the operators in the witness commute. As a result, there exists a measurement basis in which one can derive the expectation value of all these operators, reducing the number of terms to one.

When considering the qudit case, there exist states which are entangled but cannot be detected by a PPT witness (see, for example, [36,37]). These states have also been referred to

<sup>1</sup>Note that, at  $\tau = 2.5$  s, as  $D \rightarrow \infty$  the entanglement entropy converges to approximately 0.039.

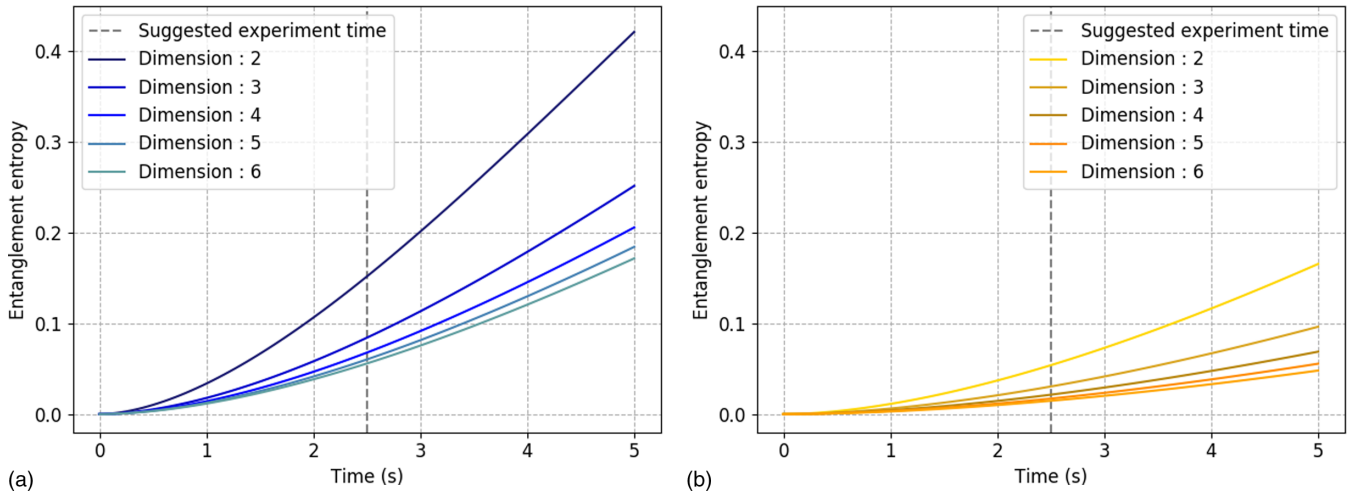


FIG. 3. Entanglement entropy scaling with the state dimension for  $D = 2-6$  for (a) the parallel setup and (b) the linear setup.

as bound entangled, and multiple methods have been developed to assess them [38–43]. The witnesses described above may therefore not be sufficient to test entanglement of  $D \otimes D$  systems (with  $D > 2$ ) as they would, by construction, fail to detect positive partial transpose entangled states (PPTESs). These can nonetheless be useful in case the theoretical density matrix of the state created by the experiment is indeed a NPT.

There is currently no general witness construction strategy for detecting PPTESs (also known as entangled bound states) and research is focused on designing witnesses specific to certain families of states. Thankfully, bound entanglement represents only a small proportion of all entangled states and remains unlikely to occur in the proposed experiment.

We computed the PPT entanglement witness expectation value for  $D$ -dimensional qudits with  $D = 2-6$ . The results are presented in Fig. 4 for both the parallel and linear cases.

The expectation value of the PPT entanglement witness is nearing  $-0.148$  at  $\tau = 2.5$  s for qubits. The witness values are slightly higher for higher-dimensional qudits, echoing the

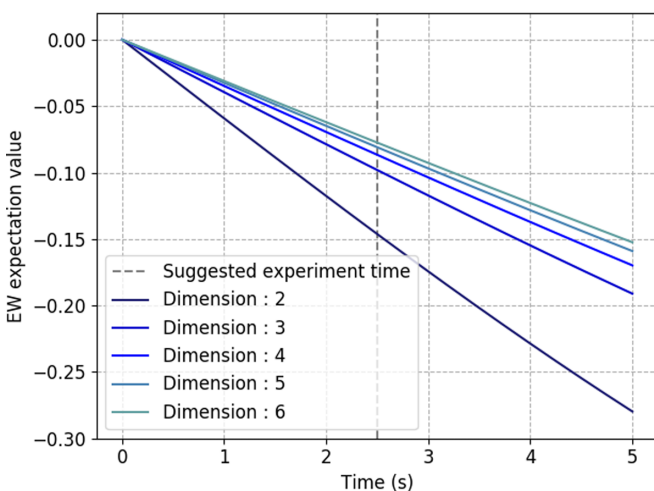


FIG. 4. Expectation value of the PPT entanglement witness for the parallel setup with state dimension for  $D = 2-6$ .

findings of the entanglement entropy test. These witnesses also appear to be finest for the set of states that are produced by each setup. A witness  $\mathcal{W}_A$  is set to be finer than another witness  $\mathcal{W}_B$  if it detects as entangled all the states detected by  $\mathcal{W}_B$  and at least one more (see Ref. [44]). In this case, the witnesses computed are clearly able to detect all entangled states produced (for any  $\tau$ ), albeit with values very close to zero for low values of  $\tau$ .

Following the above, we can also note that the high-dimension states generated by the QGEM experiment setups considered must be NPT entangled states; otherwise,  $\mathcal{W}_{\text{PPT}}$  would fail to detect them as entangled.

A further consideration regarding the entanglement witness is how many operators it needs to be broken into to be measured experimentally. For this, we can consider the scaling of generalized Gell-Mann matrices, which is a generalization of the Pauli basis to quantum states of dimensions higher than 2. There are  $D^2$  element for a set of Gell-Mann matrices for a  $D$ -dimensional quantum state. Because we build a system composed of two quantum objects, we are therefore looking at a maximum total number of operators of  $D^4$  for the entanglement witness.

We find that the entanglement witness derived from the PPT principle has, in general, a slightly lower number of operators than this (due to the weights of certain operators being negligible or equal to zero in the decomposition of the entanglement witness). We can further improve on this number by grouping together the operators that can be jointly measured. In general, operators can be jointly measured if they can be diagonalized together in a specific basis (tensor product basis) (for an overview of the method see [45]). Conveniently, this is equivalent to saying that operators can be jointly measured if they commute. Commutation is not transitive, and as such, there may be many different solutions to grouping operators together. To find a good solution, we use the largest-degree-first coloring (LDFC) algorithm (for a good summary of the LDFC algorithm, see the Supplemental Material in [46]), whereby groups are composed starting from one of the operators which have the highest number of commuting operators. The results we obtained are summarized in Table I.

TABLE I. Number of operators in the generalized Pauli decomposition of the witnesses, which must be measured to estimate the expectation value of the entanglement witness in the parallel case for  $D = 2-6$ . Column 3 presents the number of operator groups that can be jointly measured in a single basis, obtained using the LDFC algorithm. Given this algorithm is a heuristic, one could find a different set and number of groups.

$D$	PPT witness	PPT witness (grouped)
2	4	1
3	77	14
4	244	28
5	613	53
6	1272	94

One point to note is that measuring operators jointly requires finding and implementing a joint measurement basis. While straightforward in some cases, this could yield some significant complications in an actual experiment as it may require nonlocal operations.

### V. TESTING MODELS WITH DECOHERENCE

So far we have considered the case where both qubits are only coupled with each other through their positional

$$\rho_d \rightarrow \begin{bmatrix} c_{11} & c_{12}e^{-\gamma\tau} & \vdots & c_{1(d-1)}e^{-\gamma\tau} & c_{1d}e^{-\gamma\tau} \\ c_{21}e^{-\gamma\tau} & c_{22} & \vdots & c_{2(d-1)}e^{-\gamma\tau} & c_{2d}e^{-\gamma\tau} \\ \vdots & \vdots & \ddots & \vdots & \vdots \\ c_{(d-1)1}e^{-\gamma\tau} & c_{(d-1)2}e^{-\gamma\tau} & \vdots & c_{(d-1)(d-1)} & c_{(d-1)d} \\ c_{d1}e^{-\gamma\tau} & c_{d2}e^{-\gamma\tau} & \vdots & c_{d(d-1)} & c_{dd} \end{bmatrix}.$$

The overall two-qudit system density matrix is then computed using  $\rho_{\text{system}} = \rho_d^{(1)} \otimes \rho_d^{(2)}$ .

We computed the expectation value of  $\mathcal{W}_{\text{PPT}}$  for dimensions 2–6 for incremental values of  $\gamma$ . The results are plotted in Fig. 5. Interestingly, higher-dimension models appear more resilient to decoherence than the qubit case. It is worth noting that increasing decoherence in the model also reduces the optimal time for the experiment, that is, the time at which the entanglement witness is most negative, and the ability to detect entanglement with longer experiment times. To be better understand the interplay between time, decoherence, and the number of dimensions, the expected value of  $\mathcal{W}_{\text{PPT}}$  was computed at two different values for the decoherence rate: 0.1 and 0.125 Hz (see Fig. 6).

The advantage of higher-dimension models, when decoherence is increased, become significant when  $\gamma \gtrsim 0.1$  Hz. This suggests that in a real run of the experiment, multicomponent superpositions may be preferable, or even necessary if decoherence is sufficiently high. We can also observe, as expected, that longer time becomes detrimental for high decoherence rates. We also considered the problem of optimizing the experiment runtime to maximize the decoherence rate for which the entangled witness could detect the state as entangled.

superposition. A real experimental setting cannot however fully remove the potential for coupling of the studied quantum system with the environment.

The particles' coherence and hence joint entanglement erodes over time due to interaction with the environment. This results in decoherence of the positional qudits into a single, defined position or a classical mixture of differing but well-defined positions.

We schematically incorporate this in our model by adding a time-dependent exponential decay to all off-diagonal terms of each qudit's density matrix, parametrized by the decoherence rate  $\gamma$ . This is under the assumption that in any experiment  $\frac{\Delta x}{D} \gg \lambda_{\text{dB}}$ , where  $\lambda_{\text{dB}}$  is the mass's de Broglie wavelength. For a generic qudit, with dimension  $D$  and density matrix  $\rho_d$ , we can write

$$\rho_d = \begin{bmatrix} c_{11} & c_{12} & \vdots & c_{1(d-1)} & c_{1d} \\ c_{21} & c_{22} & \vdots & c_{2(d-1)} & c_{2d} \\ \vdots & \vdots & \ddots & \vdots & \vdots \\ c_{(d-1)1} & c_{(d-1)2} & \vdots & c_{(d-1)(d-1)} & c_{(d-1)d} \\ c_{d1} & c_{d2} & \vdots & c_{d(d-1)} & c_{dd} \end{bmatrix};$$

as such, following the model described above, decoherence is incorporated as

$$\begin{bmatrix} c_{11} & c_{12}e^{-\gamma\tau} & \vdots & c_{1(d-1)}e^{-\gamma\tau} & c_{1d}e^{-\gamma\tau} \\ c_{21}e^{-\gamma\tau} & c_{22} & \vdots & c_{2(d-1)}e^{-\gamma\tau} & c_{2d}e^{-\gamma\tau} \\ \vdots & \vdots & \ddots & \vdots & \vdots \\ c_{(d-1)1}e^{-\gamma\tau} & c_{(d-1)2}e^{-\gamma\tau} & \vdots & c_{(d-1)(d-1)} & c_{(d-1)d} \\ c_{d1}e^{-\gamma\tau} & c_{d2}e^{-\gamma\tau} & \vdots & c_{d(d-1)} & c_{dd} \end{bmatrix}.$$

In Appendix C we plot the expectation value of  $\mathcal{W}_{\text{PPT}}$  for different values of  $\tau$ , including decoherence. The result is that  $\tau = 2.5$  s is nearly optimal for qubits and qudits, though shorter time performs marginally better for the latter. Of course the experiment can be run for shorter times without any negative impacts provided a detectable level of entanglement has developed.

While higher-dimension setups are more resilient to decoherence, one key question in this analysis is to determine what number of measurements will be required to reject that the experiment state is not entangled. In order to further this analysis, we now need to fully simulate the experiment in order to determine the required number of measurements and runtime of the QGEM experiment. This is the object of the next section.

### VI. EXPERIMENT SIMULATION

In this section we present experiment simulations used to estimate the number of measurements that will be required to reject the hypothesis that the qubit pair is not entangled.

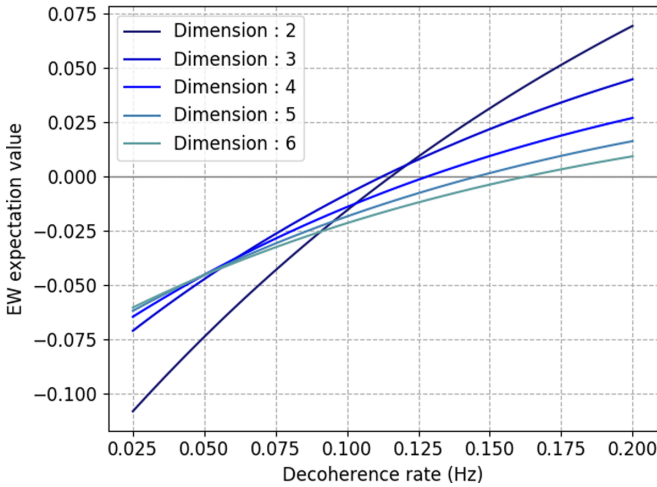


FIG. 5. Expectation value of the PPT entanglement witness as a function of the decoherence rate in the parallel setup and with  $D$  ranging from 2 to 6.

Failure to reject only means that it is impossible at this stage to confidently test for gravitationally mediated entanglement.

To compare the entanglement witnesses and the different models proposed, we simulate an experiment as described below.

(i) The entanglement witness is decomposed into a weighted sum of generalized Pauli tensor terms (Gell-Mann matrices for qutrits and generalized  $d$  dimension Pauli operators for qudits; we used the method for generalization of Pauli operators described in Ref. [47]). In some cases, we group the operators (following the groups described in Table I).

(ii) The quantum state resulting from the experiment is measured a predetermined number of times against each of the Pauli terms or group to compute (a) their expectation value and (b) the standard error of the measurement series. To minimize the variance of the observable for a given number of measurements, we have weighted the number of measurements in proportion to the weight of each Pauli tensor terms (or group) in the decomposition of the witness.

(iii) Details on how confidence levels are computed can be found in Appendix D.

The plots presented in this section are an average over many single runs of each numerical experiment simulation. As such, these should be representative of a typical run of the experiment. The conclusions drawn from these are only meant to indicate the order of magnitude of the number of measurements required in order to define the most adequate experiment setup.

We first describe the results obtained from the experiment simulation with qubits. The simulation is first run comparing the linear and parallel setups with no decoherence in Fig. 7 followed by plots of the simulation for increasing decoherence rate  $\gamma$  in Fig. 8. We have used  $\mathcal{W}_{\text{PPT}}$  with full basis decomposition in this first experiment simulations, holding  $\Delta x = 250 \mu\text{m}$  and  $\tau = 2.5 \text{ s}$ .

As we can see from Fig. 7, with no decoherence, it takes about 500 measurements to reject the hypothesis that the two states are not entangled at a 99.9% confidence level in the parallel case and at least 3000 measurements for the linear setup.

Using the witness derived in the parallel setup marginally improves the results of the linear case, although not sufficiently for it to be comparable to the parallel version of the experiment. This further confirms that the parallel setup will be preferable in a real experiment and we therefore discard the linear setup in the remainder of the simulations.

We can expect that incorporating decoherence will increase the number of measurements required as it pushes the expectation value of  $\mathcal{W}_{\text{PPT}}$  upward. The results of the qubit experiment simulations with decoherence are presented in Fig. 8, which illustrates the rapid increase in the number of measurements required as the decoherence rate is raised. For  $\gamma = 0.05 \text{ Hz}$ , the parallel setup still only requires about 2000 measurements. This figure goes up to approximately 6000 measurements for  $\gamma = 0.075 \text{ Hz}$ . At  $\gamma = 0.1 \text{ Hz}$ , the experiment would require at least 25 000 measurements. At this decoherence rate, qubits have lower negative expectation values for  $\mathcal{W}_{\text{PPT}}$  than some qudits, and at decoherence rate above  $\gamma = 0.12 \text{ Hz}$ , the expectation value of the witness is positive (that is, no entanglement is detected and therefore the results are not plotted).

We repeated the experiment simulations as described above with differing decoherence rates in the case of qudits. We have used the  $D = 6$  qudit case for illustration. As for the qubit simulations, all the experiments use the parallel setup,  $\Delta x = 250 \mu\text{m}$  and  $\tau = 2.5 \text{ s}$ .

As expected, for the six-qudit case, the number of measurements required is significantly higher. This is primarily due to the large number of additional terms to compute. Our results are presented in Fig. 9 and show that for  $\gamma = 0.05 \text{ Hz}$ , over 200 000 measurements would be needed, while nearly 400 000 would be required if  $\gamma = 0.075 \text{ Hz}$  and about 600 000 for  $\gamma = 0.1 \text{ Hz}$ .

One last test that is worth considering is the situation in which grouping of terms is allowed (this is subject to being able to produce the relevant measurement bases experimentally, as mentioned in Sec. IV). Figure 10 presents the results in the case of qubits. We can already see the drastic reduction in the total number of measurements required, resulting from the reduction of terms to measure from 4 (in reality 3 since the identity term does not need to be measured) to 1. Fewer than 1000 measurements and 2000 measurements are necessary when  $\gamma = 0.05$  and  $0.075 \text{ Hz}$ , respectively. Similarly, only about 12 000 measurements are required if  $\gamma = 0.1 \text{ Hz}$ .

A very similar pattern can be seen in the qudit case. The results for six qudits are presented in Fig. 11. The number of measurements is drastically reduced when operators are grouped. About 25 000 measurements are needed for  $\gamma = 0.05 \text{ Hz}$ , while  $\gamma = 0.075 \text{ Hz}$  requires fewer than 40 000 measurements and  $\gamma = 0.1 \text{ Hz}$  fewer than 80 000.

There are clearly no reasons to use high-dimensional qudits unless the decoherence rate is such that the entanglement witness for qubits always has a positive expectation value. In the experiment settings we have assumed, this happens at about  $\gamma \approx 0.12 \text{ Hz}$ . We therefore present in Fig. 12 an experiment simulation showing how six qudits perform in the window of decoherence rate in which high-dimensional qudits become relevant.

At  $\gamma = 1.25 \text{ Hz}$ , it is clear that the six-qudit states still require a very large number of measurements in order to

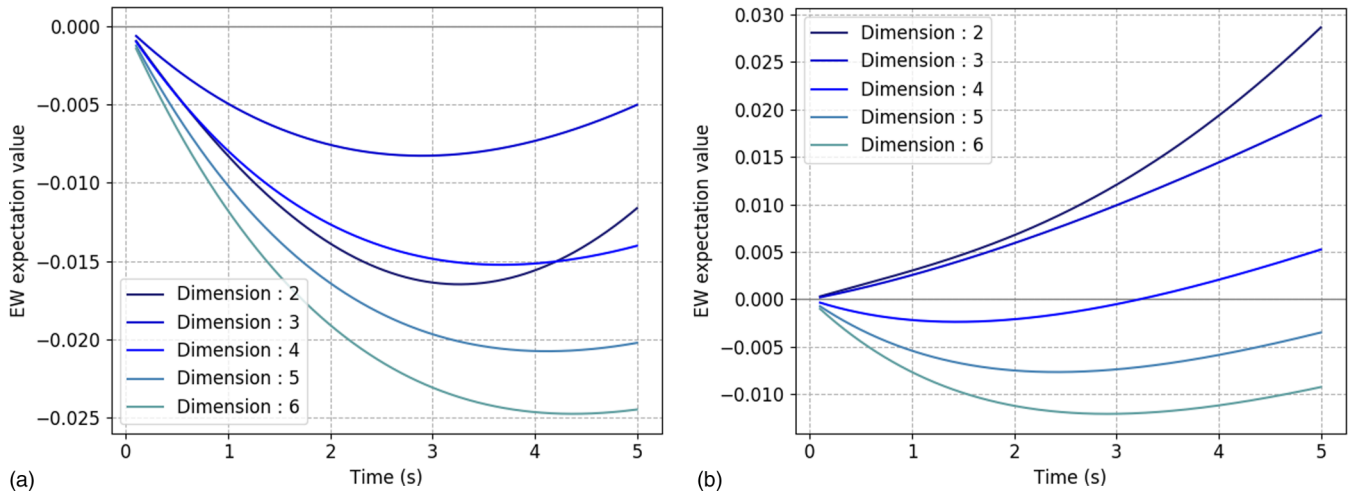


FIG. 6. Entanglement witness expectation value over time for the parallel setup and with  $D$  ranging from 2 to 6: (a)  $\gamma = 0.1$  Hz and (b)  $\gamma = 0.125$  Hz.

reject the null hypothesis. However, grouping the operators to measure in joint measurement bases allows reducing the number of measurements required from nearly 2 000 000 to slightly above 200 000. It is worth noting that at this rate, the qubit case would not work as decoherence pushes the expectation value of the witness above zero and the four-qudit and five-qudit cases are too close to zero to reach confidence of 99.9% in a realistic number of measurements.

VII. CONCLUSION

This paper considered modifying the setup proposed in the original QGEM experiments to determine how best to generate, protect, and detect entanglement in a future experiment. We looked at two aspects, the geometric setup of the experiment and the number of dimensions of the quantum objects

used, and developed a generalized mathematical model of the experiment.

Based on this model and using entanglement entropy, we concluded that the parallel-qubit setup generates entanglement the fastest for realistic experiment runtimes ( $\tau$  of order of 1 s). As entanglement entropy cannot account for entanglement once decoherence is introduced, we presented an entanglement test based on entanglement witnesses. We concluded that as the decoherence rate is increased to higher dimension, qudits finally outperform qubits by providing lower expectation values for the witnesses.

To estimate which setup would require the fewest measurements to evidence entanglement, we simulated experiments to define a confidence level for the negativity of the expectation value of the witness given a certain number of measurements. Without noise, at a 99.9% certainty level, the parallel-qubit

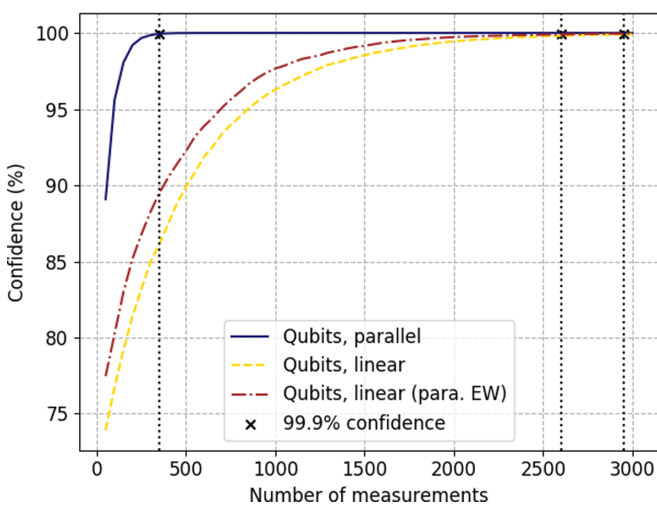


FIG. 7. QGEM experiment simulation in the linear and parallel setups (no decoherence). There is the expected level of confidence (probability of the witness value actually being negative) in the qubit case. We added the case in which the parallel witness is used for the linear setup showcasing the benefits of having a lower number of terms to compute.

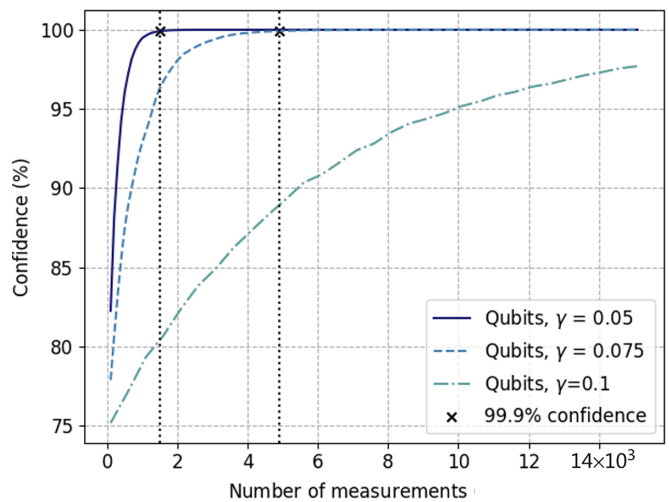


FIG. 8. QGEM experiment simulation with qubits. The confidence levels for three decoherence levels (0.05, 0.075, and 0.1 Hz) are shown as a function of the number of measurements available. Here the witness has expectation values of  $-0.074$ ,  $-0.043$ , and  $-0.016$ , respectively.

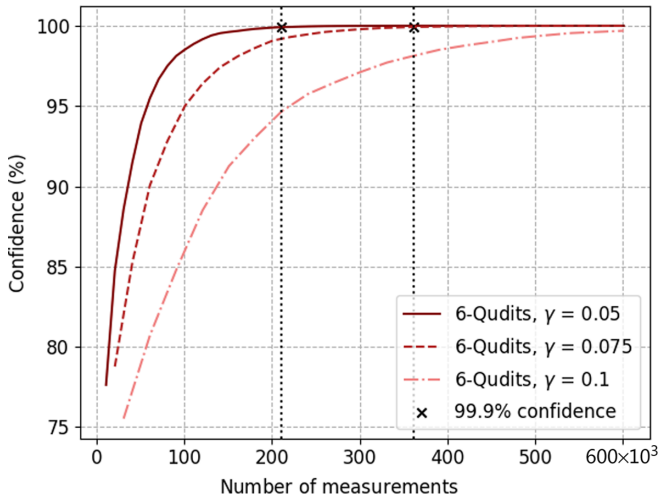


FIG. 9. QGEM experiment simulation with six qudits. The confidence levels for three decoherence levels (0.05, 0.075, and 0.1 Hz) are shown as a function of the number of measurements available. Here the witness has expectation values of  $-0.045$ ,  $-0.032$ , and  $-0.021$ , respectively

setup requires fewer than 2000 measurements (1000 when grouped) to reject the null hypothesis (that the state is not entangled). The number of measurements required increases rapidly when decoherence is introduced.

Qudits of higher dimensions only become more useful than qubits when the expectation value of the witness for qubits becomes non-negative. That is because the number of basis elements to be estimated to calculate the witness expectation value increases quadratically in the number of dimensions ( $d^4$ ). In the experiment settings proposed, at  $\tau = 2.5$  s and  $\Delta x = 250$   $\mu\text{m}$ , qudits of dimension 6 are more favorable than qubits when the decoherence rate is  $\gamma \sim 0.125$  Hz; however,

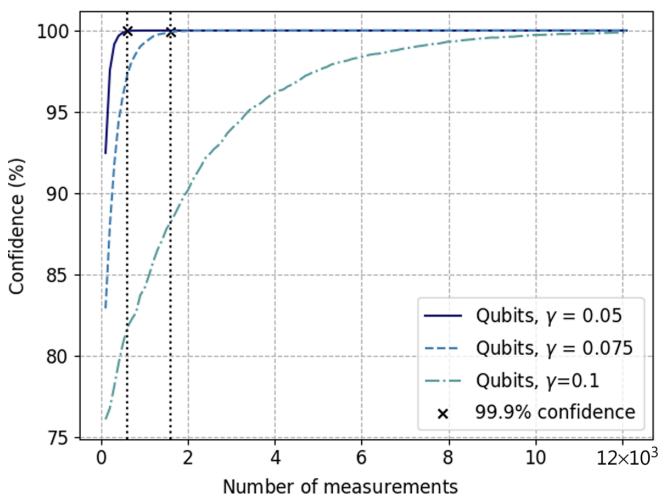


FIG. 10. QGEM experiment simulation with qubits (operators grouped). The confidence levels for three decoherence levels (0.05, 0.075, and 0.1 Hz) are shown as a function of the number of measurements available. Here the witness has expectation values of  $-0.074$ ,  $-0.043$ , and  $-0.016$ , respectively.

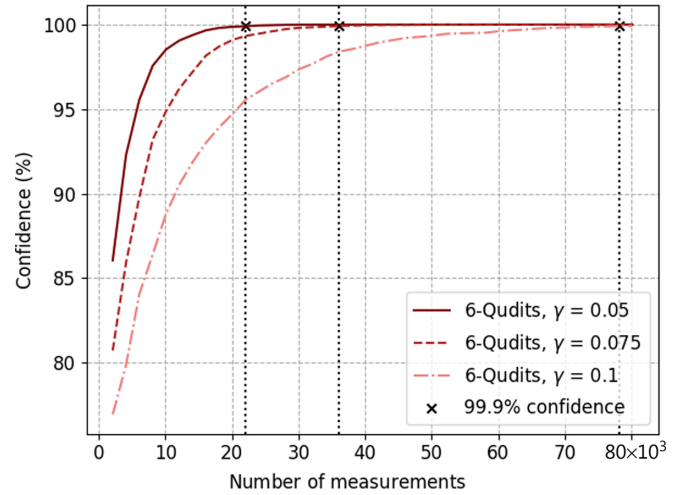


FIG. 11. QGEM experiment simulation with six qudits (operators grouped). The confidence levels for three decoherence levels (0.05, 0.075, and 0.1 Hz) are shown as a function of the number of measurements available. Here the witness has expectation values of  $-0.045$ ,  $-0.032$ , and  $-0.021$ , respectively.

in this case, over 2 000 000 measurements will be required (200 000 when operators are grouped).

Thus, to further improve the experiment design, the following points should be considered. Clearly, reducing the qudit-pair exposure to the environment to decoherence would render the experiment more economical. The total expected decoherence rates in specific, realistic experimental designs must be estimated in order to confirm whether higher-dimension qudits will be required. Finally, any increase in the superposition width  $\Delta x$  is significantly beneficial as it both improves the entanglement generation rate, allowing a significant reduction in overall runtime, which therefore also minimizes the impact of decoherence.

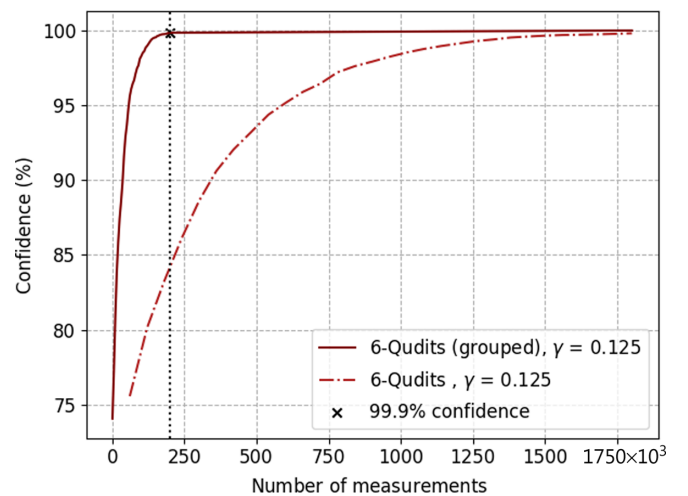


FIG. 12. QGEM experiment simulation with six qudits. The confidence levels for a decoherence rate of 0.125 Hz are shown as a function of the number of measurements available in a case where the operators are grouped and a case where they are not.



Our PYTHON model for computation and modeling of the QGEM experiment is available in [48].

**ACKNOWLEDGMENTS**

J.T. was supported by the UK EPSRC (Grant No. EP/R513143/1). R.J.M. was supported by a University College London departmental studentship. The research of A.M. was funded by the Netherlands Organization for Science and Research through Grant No. 680-91-119.

**APPENDIX A: THE GEOMETRICALLY GENERALIZED MODEL**

There are a number of parameters in the generalized formula that can be modified and tested for more effective entanglement generation. We have isolated two which offer particular insights, the superposition width  $\Delta x$  in Sec. VII and the rotation angles  $\theta_1$  and  $\theta_2$  in Sec. VII. Prior to this, however, there are a few points that are worth noting.

(i) It is clear that more time can allow achieving maximally entangled states; however, increasing the experimental runtime is unrealistic due to greater risk of decoherence. This point is covered in more detail in Sec. V.

(ii) Reducing the minimum distance  $d$  also clearly generates much faster entanglement. However, as mentioned before, this is not necessarily useful in practice. This has been considered by others [21], and any results here will also hold for such modified setups.

(iii) Using more massive quantum objects results in higher relative phases and in faster entanglement generation. However, more massive objects would also mean more challenging implementation for the interferometry, larger particle radii, and hence higher Casimir-Polder forces. This could in turn increase the minimum distance  $d$  and overall negatively impact entanglement growth. This is not something we will consider further.

**1. Comparing rotation angle setups**

In the main text we presented only the linear and parallel cases. Based on our results, the parallel setup entangles the qudits faster. For completeness, and to allow for further modification in the implementation by experimentalists, we also considered a range of additional geometries for the setup that can be implemented using the generalized QGEM model derived previously.

The heatmap presented in Fig. 13 displays the entanglement entropy for all possible combinations of  $\theta_1$  and  $\theta_2$  as defined in Fig. 2, having set  $\Delta x = 250 \mu\text{m}$  and  $\tau = 2.5 \text{ s}$ . The dark blue dots represent the two possible parallel setups  $[(\theta_1 = \frac{3\pi}{2}, \theta_2 = \frac{\pi}{2}) \text{ and } (\theta_1 = \frac{\pi}{2}, \theta_2 = \frac{3\pi}{2})]$ , while the yellow dot represents the linear setup  $(\theta_1 = \theta_2 = 0)$ . On the heatmap, blue represents low entanglement entropy while white represents entanglement entropy nearing 1.0. It appears from this figure that higher entanglement entropy could possibly be achieved with alternative setups; however, this is without considering that some combinations result in some superposition instances being under  $200 \mu\text{m}$  and therefore subject to non-negligible Casimir-Polder forces (represented by the shaded areas in the figure).

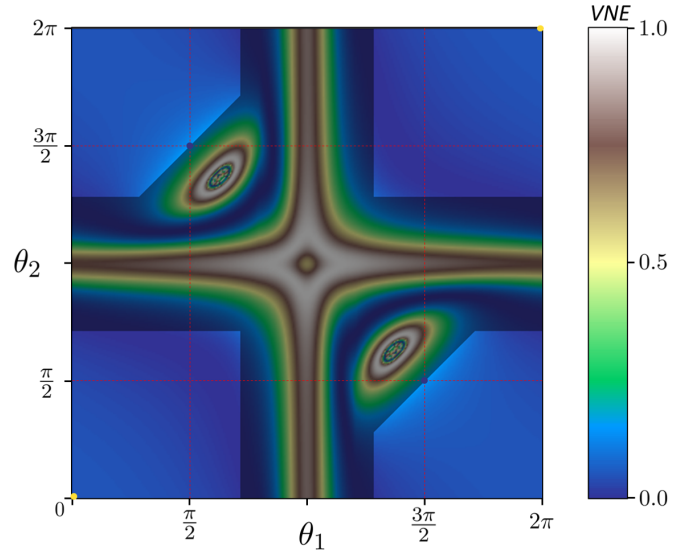


FIG. 13. Entanglement entropy for all possible combinations of  $\theta_1$  and  $\theta_2$ . The areas of reduced contrast (the region around the center +) are forbidden based on the requirement that the states do not come too close.

**2. Impact of superposition width  $\Delta x$  on entanglement entropy**

Figure 14 shows that a larger superposition width results in faster von Neumann entropy growth. To illustrate this point we can consider the phases for the parallel-qudit setup:  $\phi_{pq}$  is smaller than or equal to  $\phi$ , reaching equality at  $\Delta x = 0 \text{ m}$ ; as  $\Delta x$  increases,  $\phi_{pq}$  decreases, resulting in all the phase factors  $\Delta\phi_{pq}$  becoming more negative than they already are and as such accelerating entanglement generation.

The superposition width, however, is limited in practice by experimental considerations such as the magnetic field gradient achievable. This suggests that by further modifying the arrangement into a parallel setup one can further reduce the magnetic field gradient and/or other experimental parameters while maintaining a detectable level of entanglement.

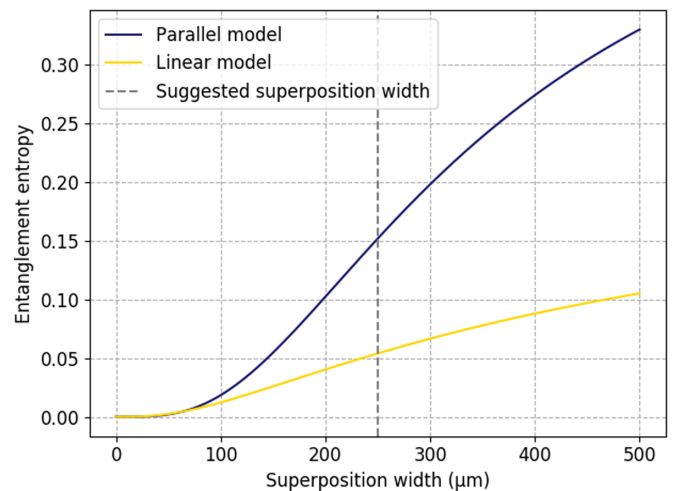


FIG. 14. Entanglement entropy for the parallel and linear setups in the qubit case as a function of the superposition width  $\Delta x$ .

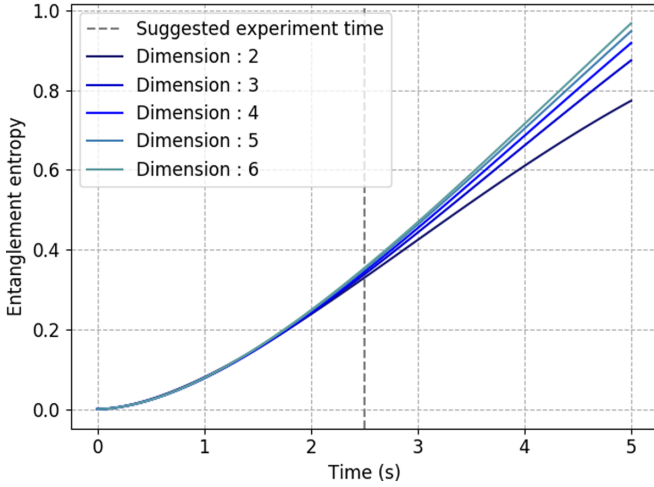


FIG. 15. Entanglement entropy as a function of time for  $D$  ranging from 2 to 6. In this case, we have scaled  $\Delta x$  to the number of dimensions.

Using higher-dimension spin quantum objects would, in theory, result in larger possible superposition width due to the spin-dependent nature of the magnetic field gradient coupling. This suggests that higher-dimensional objects would perform better than qubits if their maximum superposition width is higher. However, once a larger spin object is created, one can simply initialize the state including only the outer spin states and hence recreating a qubit state which performs better at an equivalent value of  $\Delta x$ . For illustration purposes, Fig. 15 represents a plot of entanglement entropy against time for qudits in which  $\Delta x$  is scaled to the number of dimensions. This somewhat unrealistic setup leads to higher-dimensional objects performing significantly better.

As such, the analysis allows us to conclude the following.

- (i) Qubits entangle faster than qudits for values of  $\tau$  and  $\Delta x$  realistic for the experiment.
- (ii) Parallel setups entangle faster for all dimensions.
- (iii) The superposition width  $\Delta x$  will be the variable of interest in terms of obtaining faster entanglement or a more easily implementable experiment.

#### APPENDIX B: ALTERNATIVE WITNESS: VICINITY WITNESS FOR NEGATIVE PARTIAL TRANSPOSE ENTANGLED STATES

We consider an alternative entanglement witness, which is built to detect entangled states in the vicinity of a known entangled pure state. Constructing this witness amounts to finding a value for  $\alpha$  such that  $\text{Tr}(\mathcal{W}_{\text{vic}}\rho) \geq 0$  for all separable states, with  $\mathcal{W}_{\text{vic}}$  given by

$$\mathcal{W}_{\text{vic}} = \alpha \mathbb{I} - |\psi\rangle\langle\psi|. \quad (\text{B1})$$

The maximum value of  $\alpha$  is then derived as the square of the maximum Schmidt coefficient of the pure state [49]. Denoting by  $\lambda_m$  the highest of these coefficients, we can rewrite the witness as

$$\mathcal{W}_{\text{vic}} = \lambda_m^2 \mathbb{I} - |\psi\rangle\langle\psi|. \quad (\text{B2})$$

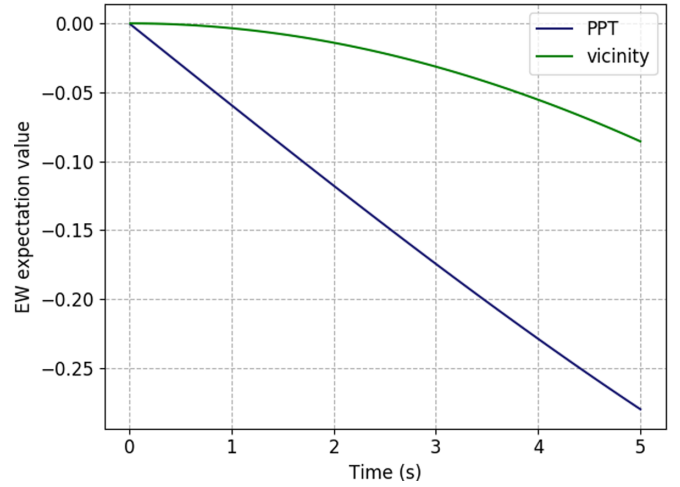


FIG. 16. Expectation value of the PPT and vicinity entanglement witnesses as a function of time in the qubit case.

We can now compare the performance of the PPT-based witness  $\mathcal{W}_{\text{PPT}}$  and the vicinity witness  $\mathcal{W}_{\text{vic}}$ . This analysis is restricted to the parallel-qubit version of the QGEM experiment as it appears to be the most optimal setup.

Comparing the expectation value of the PPT-based witness and the vicinity witness, the former exhibits clearly much lower values in short time frames (see Fig. 16). As such, it is the recommended entanglement witness for the implemented experiment. In Table II we show that the vicinity witness in general requires measuring fewer terms than the PPT witness; it is not sufficient, however, to make it more advantageous than the PPT witness in an experimental model and therefore we have mostly not included it in our analysis.

There also exist numerous other entanglement witnesses, often based on existing separability criteria, which will not be treated here as not directly relevant to the proposed research. (For an overview of several entanglement witnesses see Ref. [50]).

A possible way to reduce the number of operators to be measured would be to find a suboptimal witness with a lower number of terms to measure. One example is an approach similar to Bell inequalities, which do not detect all the entangled states as they focus only on identifying states which cannot be explained through local hidden variable (LHV) models. In [51] Hyllus *et al.* showed that it is possible to convert an

TABLE II. Number of operators to be measured to estimate the expectation value of the entanglement witness in the parallel case for  $D = 2-6$  for the parallel case and linear case using the PPT entanglement witness and for the parallel case using the vicinity entanglement witness.

$D$	PPT (parallel)	PPT (linear)	Vicinity (parallel)
2	4	9	6
3	77	81	60
4	244	256	211
5	613	625	547
6	1272	1296	1166

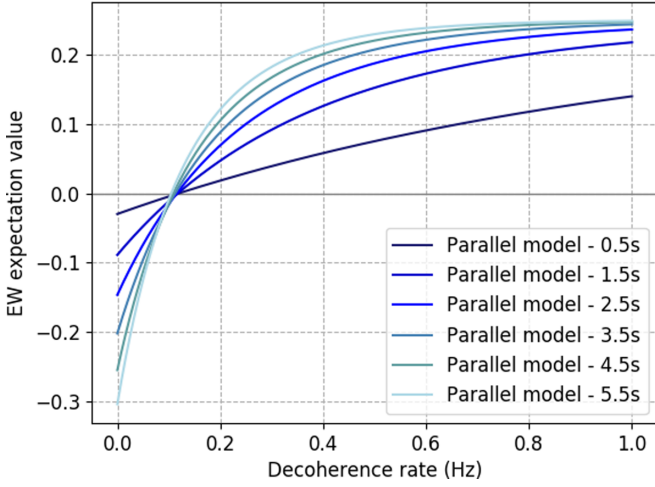


FIG. 17. Expectation value of the PPT entanglement witness for different runtimes of the experiment and as a function of the decoherence rate in the case  $D = 2$ .

optimal entanglement witness into a Clauser-Horne-Shimony-Holt (CHSH)-type inequality. The resulting inequality detects non-LHV states optimally, but not entangled LHV states.

Therefore, there is a trade-off between the optimality of the entanglement witness (the finest entanglement witness being the optimal witness for a given entanglement detection problem) and the overall number of measurements required to test entanglement. The conversion method developed by Hyllus *et al.* only relates to qubits and does not take into account the impact of decoherence on the detectability of entanglement [51]. However, for the qubit case, given the witness used only has three terms that need to be measured, CHSH-type inequalities are unlikely to provide a significant benefit.<sup>2</sup>

**APPENDIX C: TIME TRADE-OFF WITH DECOHERENCE**

In the original paper, Bose *et al.* suggested an experiment runtime of  $\tau = 2.5$  s. In this Appendix we consider a simple way to estimate which runtime produces the highest resilience to decoherence (which runtime results in the expectation value of the entanglement witness reaching 0 for the highest decoherence rate). Figure 17 presents the case of qubits, while Figure 18 presents the case of six-dimensional qudits.

Figure 17 shows that additional time has little impact on how high the decoherence rate can be allowed to be. It does however offer more negative expectation values for the entanglement witness. If the experiment decoherence rate is estimated, one can then verify whether additional time can reduce the overall number of measurements required. The effect is more pronounced in the six-dimensional qudit case as shorter times offer negative expectation values of the witness for higher decoherence rate.

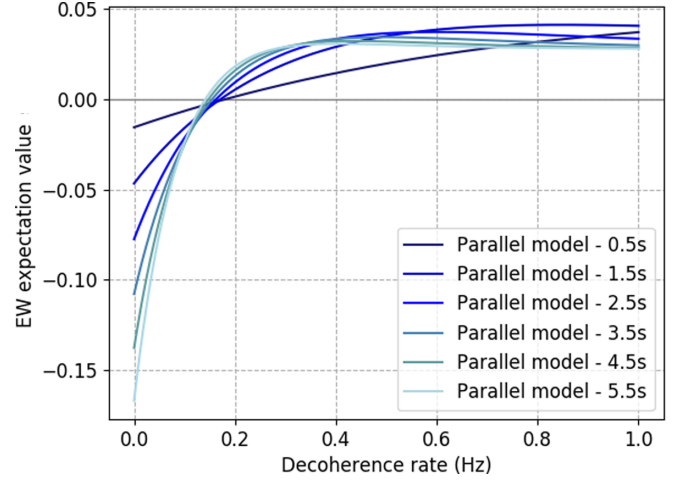


FIG. 18. Expectation value of the PPT entanglement witness for different runtimes of the experiment and as a function of the decoherence rate in the case  $D = 6$ .

**APPENDIX D: COMPUTING THE CONFIDENCE INTERVAL FOR A QUANTUM OBSERVABLE**

In order to compute statistics related to the expectation value of a quantum observable, we first need to deconstruct the witness we are trying to estimate into a weighted sum of observables that can be directly measured, i.e., a set of Pauli strings. In particular, in the case of our two-qudit system we have at most  $D^4$  terms. These terms and the tensor product consist of the list of Gell-Mann matrices of dimension  $D$  which are numbered  $\mathcal{D} = D^2$ . Any witness  $\mathcal{W}$  can then be written as

$$\mathcal{W} = \sum_i^{\mathcal{D}} \sum_j^{\mathcal{D}} c_{ij} \lambda_i^{(1)} \otimes \lambda_j^{(2)}, \tag{D1}$$

with  $\lambda$  representing any Gell-Mann matrix (in the qubit case, these are the Pauli matrices:  $\lambda \in \{\mathbb{I}, X, Y, Z\}$ ). Any tensor  $w_{ij} = \lambda_i^{(1)} \otimes \lambda_j^{(2)}$  is a quantum observable that can be directly measured in an experiment.

For a given number of measurements  $M$ , we can partially improve the overall variance of the observable by distributing these measurements in proportion to the weight of each term in the decomposition of the witness such that (noting  $c = \sum_i \sum_j |c_{ij}|$ ) we have

$$M = \sum_i \sum_j M_{ij}, \tag{D2}$$

$$M_{ij} = \frac{|c_{ij}|}{c} M. \tag{D3}$$

Considering that we conduct  $M_{ij}$  measurements, we can then determine the mean and variance of each of the term as follows:

$$\overline{w_{ij}} = \sum_m \frac{w_{ij}^{(m)}}{M_{ij}}, \tag{D4}$$

$$\sigma_{ij}^2 = \sum_m \frac{(w_{ij}^{(m)} - \overline{w_{ij}})^2}{(M_{ij} - 1)}. \tag{D5}$$

<sup>2</sup>Nguyen and Bernards provide a threshold value for the phase of the parallel setup for which it would violate CHSH inequalities, including decoherence [20]. Further research would be necessary in order to conduct a similar test for qudits.

From there, we can compute the witness's mean and variance

$$\overline{\mathcal{W}} = \sum_i^{\mathcal{D}} \sum_j^{\mathcal{D}} \sum_m^{M_{ij}} \frac{c_{ij} w_{ij}^{(m)}}{M_{ij}}, \quad (\text{D6})$$

$$\sigma_{\mathcal{W}}^2 = \sum_i^{\mathcal{D}} \sum_j^{\mathcal{D}} \sum_m^{M_{ij}} |c_{ij}|^2 \sigma_{ij}^2. \quad (\text{D7})$$

Finally, denoting by  $\mathcal{M}$  the average number of measurements per term, we can compute the standard error of normally distributed measurement population as

$$s_{\mathcal{W}} = \frac{\sigma_{\mathcal{W}}}{\sqrt{\mathcal{M}}}. \quad (\text{D8})$$

We then compute the confidence interval  $\mathcal{C}$  as

$$\mathcal{C}_{\mathcal{W}} = [\overline{\mathcal{W}} - \alpha s_{\mathcal{W}}, \overline{\mathcal{W}} + \alpha s_{\mathcal{W}}], \quad (\text{D9})$$

with  $\alpha$  the  $t$  value corresponding to the desired level of confidence.

For computation of the confidence level, we test against the null hypothesis  $\mathcal{W} \geq \mu_0$ , with  $\mu_0 = 0$ , and compute the  $t$  values following the traditional methods for a one-sided  $t$  test:

$$t = \frac{|\mathcal{W} - \mu_0|}{s_{\mathcal{W}}}. \quad (\text{D10})$$

Confidence is then computed as  $1 - p$ , with  $p$  the  $p$  value corresponding to the  $t$  value obtained.

- 
- [1] C. Kiefer, *Quantum Gravity* (Cambridge University Press, Cambridge, 2012).
- [2] R. Colella, A. Overhauser, and S. Werner, Observation of Gravitationally Induced Quantum Interference, *Phys. Rev. Lett.* **34**, 1472 (1975).
- [3] V. Nesvizhevsky, A. Petoukhov, H. Borner, K. Protasov, A. Voronin, A. Westphal, S. Baessler, H. Abele, and A. Gagarski, Reply to ‘‘Comment on ‘Measurement of quantum states of neutrons in the Earth’s gravitational field’ ’’, *Phys. Rev. D* **68**, 108702 (2003).
- [4] B. A. Stickler, B. Papendell, S. Kuhn, B. Schriniski, J. Millen, M. Arndt, and K. Hornberger, Probing macroscopic quantum superpositions with nanorotors, *New J. Phys.* **20**, 122001 (2018).
- [5] I. Pikovski, M. R. Vanner, M. Aspelmeyer, M. S. Kim, and Č. Brukner, Probing Planck-scale physics with quantum optics, *Nat. Phys.* **8**, 393 (2012).
- [6] T. Krisnanda, G. Y. Tham, M. Paternostro, and T. Paterek, Observable quantum entanglement due to gravity, *npj Quantum Inf.* **6**, 12 (2020).
- [7] R. Howl, R. Penrose, and I. Fuentes, Exploring the unification of quantum theory and general relativity with a Bose-Einstein condensate, *New J. Phys.* **21**, 043047 (2019).
- [8] M. Carlesso, A. Bassi, M. Paternostro, and H. Ulbricht, Testing the gravitational field generated by a quantum superposition, *New J. Phys.* **21**, 093052 (2019).
- [9] N. Altamirano, P. Corona-Ugalde, R. B. Mann, and M. Zych, Gravity is not a pairwise local classical channel, *Class. Quantum Grav.* **35**, 145005 (2019).
- [10] R. J. Marshman, A. Mazumdar, G. W. Morley, P. F. Barker, S. Hoekstra, and S. Bose, Mesoscopic interference for metric and curvature and gravitational wave detection, *New J. Phys.* **22**, 083012 (2020).
- [11] D. N. Page and C. D. Geilker, Indirect Evidence for Quantum Gravity, *Phys. Rev. Lett.* **47**, 979 (1981).
- [12] A. Ashoorioon, P. B. Dev, and A. Mazumdar, Implications of purely classical gravity for inflationary tensor modes, *Mod. Phys. Lett. A* **29**, 1450163 (2014).
- [13] R. J. Marshman, A. Mazumdar, and S. Bose, Locality and entanglement in table-top testing of the quantum nature of linearized gravity, *Phys. Rev. A* **101**, 052110 (2020).
- [14] S. Bose, A. Mazumdar, G. W. Morley, H. Ulbricht, M. Toroš, M. Paternostro, A. A. Geraci, P. F. Barker, M. S. Kim, and G. Milburn, Spin Entanglement Witness for Quantum Gravity, *Phys. Rev. Lett.* **119**, 240401 (2017).
- [15] C. Marletto and V. Vedral, Gravitationally Induced Entanglement between Two Massive Particles is Sufficient Evidence of Quantum Effects in Gravity, *Phys. Rev. Lett.* **119**, 240402 (2017).
- [16] A. Belenchia, R. M. Wald, F. Giacomini, E. Castro-Ruiz, Č. Brukner, and M. Aspelmeyer, Quantum superposition of massive objects and the quantization of gravity, *Phys. Rev. D* **98**, 126009 (2018).
- [17] M. Christodoulou and C. Rovelli, On the possibility of experimental detection of the discreteness of time, *Front. Phys.* **8**, 207 (2020).
- [18] R. Howl, V. Vedral, D. Naik, M. Christodoulou, C. Rovelli, and A. Iyer, Non-Gaussianity as a signature of a quantum theory of gravity, *PRX Quantum* **2**, 010325 (2021).
- [19] H. Chevalier, A. J. Paige, and M. S. Kim, Witnessing the nonclassical nature of gravity in the presence of unknown interactions, *Phys. Rev. A* **102**, 022428 (2020).
- [20] H. C. Nguyen and F. Bernards, Entanglement dynamics of two mesoscopic objects with gravitational interaction, *Eur. Phys. J. D* **74**, 69 (2020).
- [21] T. W. van de Kamp, R. J. Marshman, S. Bose, and A. Mazumdar, Quantum gravity witness via entanglement of masses: Casimir screening, *Phys. Rev. A* **102**, 062807 (2020).
- [22] M. Toroš, T. W. van de Kamp, R. J. Marshman, M. S. Kim, A. Mazumdar, and S. Bose, Relative acceleration noise mitigation for nanocrystal matter-wave interferometry: Applications to entangling masses via quantum gravity, *Phys. Rev. Research* **3**, 023178 (2021).
- [23] D. Miki, A. Matsumura, and K. Yamamoto, Entanglement and decoherence of massive particles due to gravity, *Phys. Rev. D* **103**, 026017 (2021).
- [24] A. Matsumura and K. Yamamoto, Gravity-induced entanglement in optomechanical systems, *Phys. Rev. D* **102**, 106021 (2020).
- [25] S. A. Haine, Searching for signatures of quantum gravity in quantum gases, *New J. Phys.* **23**, 033020 (2021).
- [26] M. P. Blencowe, Effective Field Theory Approach to Gravitationally Induced Decoherence, *Phys. Rev. Lett.* **111**, 021302 (2013).

- [27] S. Rijavec, M. Carlesso, A. Bassi, V. Vedral, and C. Marletto, Decoherence effects in non-classicality tests of gravity, *New J. Phys.* **23**, 043040 (2021).
- [28] M. Toroš, A. Mazumdar, and S. Bose, Loss of coherence of matter-wave interferometer from fluctuating graviton bath, [arXiv:2008.08609](https://arxiv.org/abs/2008.08609).
- [29] D. E. Bruschi and F. K. Wilhelm, Self gravity affects quantum states, [arXiv:2006.11768](https://arxiv.org/abs/2006.11768).
- [30] L. H. Ford and T. A. Roman, Negative energy density in superposition and entangled states, *Phys. Rev. D* **77**, 045018 (2008).
- [31] C. Anastopoulos and B. L. Hu, A master equation for gravitational decoherence: Probing the textures of spacetime, *Class. Quantum Grav.* **30**, 165007 (2013).
- [32] Y. Margalit, O. Dobkowski, Z. Zhou, O. Amit, Y. Japha, S. Moukouri, D. Rohrlach, A. Mazumdar, S. Bose, C. Henkel, and R. Folman, Realization of a complete Stern-Gerlach interferometer: Towards a test of quantum gravity, *Sci. Adv.* **7**, eabg2879 (2021).
- [33] T. Biswas, E. Gerwick, T. Koivisto, and A. Mazumdar, Towards Singularity and Ghost Free Theories of Gravity, *Phys. Rev. Lett.* **108**, 031101 (2012).
- [34] T. Biswas, A. Mazumdar, and W. Siegel, Bouncing universes in string-inspired gravity, *J. Cosmol. Astropart. Phys.* **03** (2006) 009.
- [35] I. Bengtsson and K. Życzkowski, *Geometry of Quantum States: An Introduction to Quantum Entanglement* (Cambridge University Press, Cambridge, 2006).
- [36] P. Horodecki, Separability criterion and inseparable mixed states with positive partial transposition, *Phys. Lett. A* **232**, 333 (1997).
- [37] P. Horodecki, M. Horodecki, and R. Horodecki, Bound Entanglement Can Be Activated, *Phys. Rev. Lett.* **82**, 1056 (1999).
- [38] M. Horodecki, P. Horodecki, and R. Horodecki, Mixed-State Entanglement and Distillation: Is There a Bound Entanglement in Nature? *Phys. Rev. Lett.* **80**, 5239 (1998).
- [39] S. Yu and N.-L. Liu, Entanglement Detection by Local Orthogonal Observables, *Phys. Rev. Lett.* **95**, 150504 (2005).
- [40] O. Gühne, M. Mechler, G. Toth, and P. Adam, Entanglement criteria based on local uncertainty relations are strictly stronger than the computable cross norm criterion, *Phys. Rev. A* **74**, 010301(R) (2006).
- [41] D. Chruściński and A. Kossakowski, Circulant states with positive partial transpose, *Phys. Rev. A* **76**, 032308 (2007).
- [42] O. Chruscinski and A. Rutkowski, Entanglement witnesses for  $d \otimes d$  systems and new classes of entangled qudit states, *Eur. Phys. J. D* **62**, 273 (2011).
- [43] O. Rudolph, On the cross norm criterion for separability, *J. Phys. A: Math. Gen.* **36**, 21 (2003).
- [44] M. Lewenstein, B. Kraus, J. I. Cirac, and P. Horodecki, Optimization of entanglement witnesses, *Phys. Rev. A* **62**, 052310 (2000).
- [45] P. Gokhale, O. Angiuli, Y. Ding, K. Gui, T. Tomesh, M. Suchara, M. Martonosi, and F. T. Chong, Minimizing state preparations in variational quantum eigensolver by partitioning into commuting families, [arXiv:1907.13623](https://arxiv.org/abs/1907.13623).
- [46] I. Hamamura and T. Imamichi, Efficient evaluation of quantum observables using entangled measurements, *npj Quantum Inf.* **6**, 56 (2020).
- [47] R. T. Thew, K. Nemoto, A. G. White, and W. J. Munro, Qudit quantum state tomography, *Phys. Rev. A* **66**, 012303 (2002).
- [48] [https://github.com/JT76/Generalised\\_QGEM](https://github.com/JT76/Generalised_QGEM).
- [49] M. Bourennane, M. Eibl, C. Kurtsiefer, S. Gaertner, H. Weinfurter, O. Gühne, P. Hyllus, D. Bruß, M. Lewenstein, and A. Sanpera, Experimental Detection of Multipartite Entanglement using Witness Operators, *Phys. Rev. Lett.* **92**, 087902 (2004).
- [50] O. Gühne and G. Tóth, Entanglement detection, *Phys. Rep.* **474**, 1 (2009).
- [51] P. Hyllus, O. Gühne, D. Bruß, and M. Lewenstein, Relations between entanglement witnesses and Bell inequalities, *Phys. Rev. A* **72**, 012321 (2005).